Chemistry–A European Journal
Research Article
doi.org/10.1002/chem.202302619
Chemistry Europe
European Chemical Societies Publishing
www.chemeurj.org

Special Collection

Tuning the Optical Properties Through Hydrogen Bond-assisted H-aggregate Formation: The ODIN Case

Francesco Bertocchi,[a] Danilo Marchetti,[a, b] Sandra Doria,[c, d] Mariangela di Donato,[c, d] Cristina Sissa,[a] Mauro Gemmi,[b] Enrico Dalcanale,[a] Roberta Pinalli,*[a] and Andrea Lapini*[a, d]

Dedicated to Prof. Maurizio Prato on the occasion of his 70th birthday.

The current work focuses on the investigation of two functionalized naphthyridine derivatives, namely ODIN-EtPh and ODIN-But, to gain insights into the hydrogen bond-assisted H-aggregate formation and its impact on the optical properties of ODIN molecules. By employing a combination of X-ray and electron crystallography, absorption and emission spectroscopy, time resolved fluorescence and ultrafast pump-probe spectroscopy (visible and infrared) we unravel the correlation between the structure and light-matter response, with a particular emphasis on the influence of the polarity of the surrounding environment. Our experimental results and simulations confirm that in polar and good hydrogen-bond acceptor solvents (DMSO), the formation of dimers for ODIN derivatives is strongly inhibited. The presence of a phenyl group linked to the ureidic unit favors the folding of ODIN derivatives (forming an intramolecular hydrogen bond) leading to the stabilization of a charge-transfer excited state which almost completely quenches its fluorescence emission. In solvents with a poor aptitude for forming hydrogen bonds, the formation of dimers is favored and gives rise to H aggregates, with a consequent considerable reduction in the fluorescence emission. The urea-bound phenyl group furtherly stabilizes the dimers in chloroform.

Introduction

The manipulation of intermolecular interactions represents a widely explored strategy for tuning the optical properties of supramolecular structures formed by independent molecular units.[1,2] Various approaches have been employed in this endeavor, including the introduction of suitable substituents to optimize steric hindrance[3,4] and the precise control of the distance and positioning of the molecular units.[5] Chromophore aggregation is a well-known approach to adjust the optical properties of materials, particularly when medium-strong intermolecular dipole-dipole coupling is involved.[6–8] Such coupling gives rise to the formation of exciton molecular aggregates. However, while exciton molecular aggregates are easily formed through weak intermolecular interactions between molecules possessing an extended distribution of π-electrons, such as Van der Waals and stacking interactions,[9–13] they provide limited control over the conformational geometry of the aggregate. To gain precise control over the coupling between chromophores and manipulate their absorption and fluorescence properties, it is essential to control the geometry of the aggregate. This can be achieved using a wide palette of directional weak interactions, among which H-bonding is one of the preferred options.[6,9] Hydrogen bonds offer the advantage of maximizing interactions in specific directions while minimizing them in other directions.[7,14] Furthermore, hydrogen bonds can be exploited in a multiple bonding strategy to leverage the chelate cooperative effect,[15] leading to a preferential network formation among certain hydrogen interactions over others.[16,17] The precise arrangement of donors (D) and acceptors (A) in complementary units can further increase the strength of the resulting H-bond pattern,[18] according to the Jorgensen rules.[19]

In general, the formation of a new molecular aggregate, composed of two or more coupled molecules, results in the emergence of new electronic states that are delocalized across

[a] F. Bertocchi, D. Marchetti, Prof. C. Sissa, Prof. E. Dalcanale, Prof. R. Pinalli, Dr. A. Lapini
Department of Chemistry, Life Sciences and Environmental Sustainability
University of Parma, and INSTM, UdR Parma
Parco Area delle Scienze17/A, 43124 Parma (Italy)
E-mail: roberta.pinalli@unipr.it
andrea.lapini@unipr.it
[b] D. Marchetti, Dr. M. Gemmi
Istituto Italiano di Tecnologia, Center for Materials Interfaces, Electron Crystallography
Viale Rinaldo Piaggio 34, 56025, Pontedera (Italy)
[c] Dr. S. Doria, Dr. M. di Donato
ICCOM-CNR
via Madonna del Piano 10, I-50019 Sesto Fiorentino (FI) (Italy)
[d] Dr. S. Doria, Dr. M. di Donato, Dr. A. Lapini
LENS (European Laboratory for Non-Linear Spectroscopy)
Via N. Carrara 1, 5001 Sesto Fiorentino, FI (Italy)

Supporting information for this article is available on the WWW under https://doi.org/10.1002/chem.202302619

This article is part of a joint Special Collection in honor of Maurizio Prato.

all the involved molecules. These states arise from the in-phase or anti-phase combination of the excited states of the individual molecules. Moreover, depending on the sign of the coupling constant between molecular units, two distinct types of interaction can occur. In case of negative coupling constant, the in-phase combination has the lowest energy, while for positive coupling constant, the out-of-phase combination exhibits lower energy. These types of interaction give rise to J and H excitonic aggregates, respectively. J aggregates are characterized by having the lowest energy state as the optically permitted one, while H aggregates often exhibit low fluorescence emission due to the optically dark nature of their lowest energy excited state .[9]

In a previous work, we reported the design and synthesis of a functionalized naphthyridine unit, named ODIN, which possesses the ability to self-dimerize through six intermolecular hydrogen bonds, forming a DDADA bonding motif, in which two H-bonds are bifurcated.[20] We demonstrated the self-dimerization of ODIN in the solid state through X-ray crystal structure analysis, providing insights into its supramolecular arrangement. Furthermore, we successfully incorporated ODIN into a polyolefin matrix to create a dynamic cross-linked polyethylene material, where ODIN acts as a physical cross-linker.[20] Subsequent investigations focused on studying the tendency of ODIN to tautomerize, self-dimerize, or form intramolecular hydrogen bonding, and the role played by solvents in favoring inter- or intra-hydrogen bond formation.[21] However, a comprehensive rationalization of the interplay between the structural and optical properties, with a clear reference to the intermolecular interactions, is still missing. Therefore, the objective of the present work is to shed light on the correlation between the structure and light-matter response of ODIN molecules, with particular attention to the influence of the polarity of the surrounding environment.

To accomplish this, various characterization techniques were used, including X-ray crystallography, 3D electron diffraction,[22,23] UV-vis spectroscopy, fluorescence spectroscopy, time resolved fluorescence spectroscopy and ultrafast pump-probe spectroscopy. X-ray and electron crystallography allowed us to obtain precise structural information, highlighting the supramolecular arrangement and hydrogen bonding interactions of ODIN molecules, while the spectroscopic analyses let us elucidate the type of aggregates present in different solvents and the corresponding optical properties.

Results and Discussion

Two different ODIN derivatives, namely **ODIN-EtPh** and **ODIN-But**, were synthesized.[20] **ODIN-EtPh** features a butyl chain attached to the naphthyridine ring and a 4-ethylphenyl unit directly linked to the urea group (Scheme 1, left), while **ODIN-But** is characterized by a butyl chain attached to the urea group (Scheme 1, right). These derivatives were specifically designed to investigate the structural and optical properties of ODIN molecules under different solvent environments, thereby providing valuable insights into the influence of environment polarity on the hydrogen bond-assisted H-aggregate formation of ODIN.

In particular, we focused our attention on the effect of the substituent linked to the ureidic group on the stability of the intermolecular interactions. We decided to insert in one derivative a rigid group (4-Ethylphenyl group) able to limit the number of conformational degrees of freedom of the system and, possibly, to stabilize the formation of aggregates, and in the other one a small aliphatic chain, to simulate a condition very similar to that found when ODIN is linked to polymeric systems. The presence of the aliphatic chain linked to naphthyridine has the purpose of increasing the solubility of the system, quite low in the case of ODIN-EtPh. The effect of such chain related to the electronic properties of the monomer molecular system is negligible, and we also verified that the behavior of ODIN-EtPh in absence and in presence of the aliphatic side chain is identical in terms of aggregates optical properties and stability (see Supporting Information, Section 5.1 Figure S15).

Synthesis

ODIN-EtPh (Scheme S1) was obtained following our previous work,[20] while **ODIN-But** was synthetized by reacting 7-Amino-1,8-naphthyridin-2(1H)-one, prepared according to the literature,[20] with butyl isocyanate in DMF, in presence of dibutyltin dilaurate (DBTDL) as catalyst, and pyridine as base

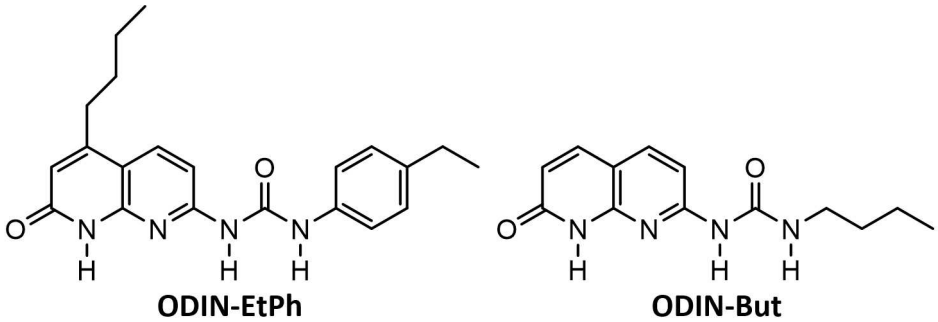

Scheme 1. Molecular structures of **ODIN-EtPh** and **ODIN-But**, both based on the 1-(7-oxo-7,8-dihydro-1,8-naphthyridin-2-yl)urea (ODIN) scaffold.

(Scheme S2). The mixture was stirred overnight at 80 °C, then cooled to room temperature and the product precipitated with hexane. The crude was filtered, washed with hexane and the final product recovered with 75% yield. **ODIN-But** was characterized via ^{1}H NMR, ^{13}C NMR and HR-ESI MS spectroscopy, and 3D electron diffraction (3D ED) analysis.

Crystallographic analysis

The solid-state characterization was carried out to investigate **ODIN** H-bond pattern in crystals grown from polar and non-polar solvents.

The **ODIN-But** crystallized from a chloroform solution exhibits thin micrometric rod-shaped crystals (Figure S4). The small crystalline domains hampered its structural analysis by single-crystal X-ray diffraction, requiring the use of 3D electron diffraction (3D ED).[22][24] Due to the sensitivity of the **ODIN-But** crystals to the electron beam, diffraction data were collected from three separate crystal areas using a special low-dose setup, in which the electron dose is below 0.05 el s^{-1} $Å^{-2}$. The diffraction patterns were recorded using a Timepix single electron detector[23] and for each crystal region, a full 3D ED experiment was performed without partial amorphization of the sample or considerable loss in diffraction data resolution.

In order to track the crystal position, while the sample is rotating, the 3D ED data have been collected in nano-diffraction mode with a particular continuous rotation (cRED) protocol, in which the parallel electron beam is not fixed in one point, but it is scanning a square area of 200 x 200 nm^2.[25] During the crystal rotation, the diffracted electrons pass through the central hole of the high-angle annular dark field (HAADF) STEM detector and are collected by the Timepix below, while the HAADF records real-time images of the scanned area, allowing live-tracking of the crystal position (Figure S5). The small size of the imaged area guarantees that the diffraction signal comes from a coherent domain. To our knowledge, this is the first time that this combined STEM-cRED data collection protocol has been successfully applied to a fully organic system. The collected diffraction data were merged, allowing for the *ab-initio* structure determination and kinematical refinement of the **ODIN-But** crystal structure (Figure S6).

The **ODIN-EtPh** crystal structure, obtained in the same crystallization conditions of **ODIN-But**, was previously published proving that in the solid state the ODIN molecules form a dimer via a sextuple H-bonding network in a DDADA fashion (CCDC Ref Code: PIWVEZ).[20] The molecular arrangements of **ODIN-But** and **ODIN-EtPh**, in crystals produced from chloroform solution, exhibit the same propensity to produce linear DDADA dimers (Figure 1). In agreement with the computational calculations, in both dimers, the ureic groups are involved in an intermolecular bifurcated N–H···O contact with the lactam C=O while the N–H of the latter in an NH···N interaction with the pyridyl ring (Table S1). Since **ODIN-But** and **ODIN-EtPh** crystal structures present an inversion centre in the middle of the **ODIN** dimer, three of the six hydrogen bonds are symmetrical equivalent.

In order to elucidate the influence of a strong H-bond acceptor solvent on the ODIN molecule conformation and its dimeric aggregation at the solid state, crystals of **ODIN-EtPh** were grown from a DMSO solution and characterized by single crystal X-ray diffraction (Figure 2). (Deposition Number(s) 1825490 (for ODIN-EtPh) contain(s) the supplementary crystallographic data for this paper. These data are provided free of charge by the joint Cambridge Crystallographic Data Centre and Fachinformationszentrum Karlsruhe Access Structures service.) The structural model shows in the asymmetric unit a DA dimer composed by two bent ODIN isomers respectively interacting with two intermolecular hydrogen bonds (Figure 2B, C). The bent form of **ODIN-EtPh** also presents an intramolecular N–H···N hydrogen bond between the ureic and pyridyl functions. The bent ODIN dimers interact at the solid state through the N3A–H···O2B and N3B–H···OAB contacts between their ureic groups, interactions that are responsible for a linear hydrogen bond network (Figure 2A). The reported crystal structure confirms that the bent ODIN isomers, also hypothesized by Loos et.al.,[21] could be generated from a polar and strong H-bond acceptor solvent such as DMSO.

Attempts to grow crystals of **ODIN-But** from a DMSO solution unfortunately failed.

Absorption emission and fluorescence relaxation properties

The optical properties of **ODIN-But** and **-EtPh** have been investigated via the help of UV-Vis absorption, steady-state fluorescence, time-resolved fluorescence, femtosecond transient absorption both in the visible and in the infrared spectral range. As already reported,[20] ODIN has a well-documented tendency to establish intermolecular hydrogen bonds giving rise to a maximum of 6 intermolecular hydrogen bond interactions in a bi-molecular structure (Figure 1E).[20] Here, our attention is focused on how the solvent polarity and capability to donate or accept hydrogen bonds influences the aggregation status and, consequently, ODIN's spectroscopic properties. Absorption and emission spectra are expected to be very sensitive probes of intermolecular interactions,[26,27] but to fulfill a complete understanding of the aggregation status and its consequences on photo-physics, ultrafast transient absorption spectroscopy, transient infrared spectroscopy and quantum chemical calculations (density functional level of theory, DFT) have been used. DMSO and $CHCl_3$ have been chosen as solvents, respectively representing a polar and highly prone to accept hydrogen bonds environment and a scarcely polar and poorly capable of forming hydrogen bonds environment.

UV-Vis and emission spectra: probing the presence of aggregates in $CHCl_3$

Absorption and steady state emission spectra of **ODIN-EtPh** and **ODIN-But** have been recorded in DMSO and $CHCl_3$ and are reported in Figure 3 and summarized in Table 1.

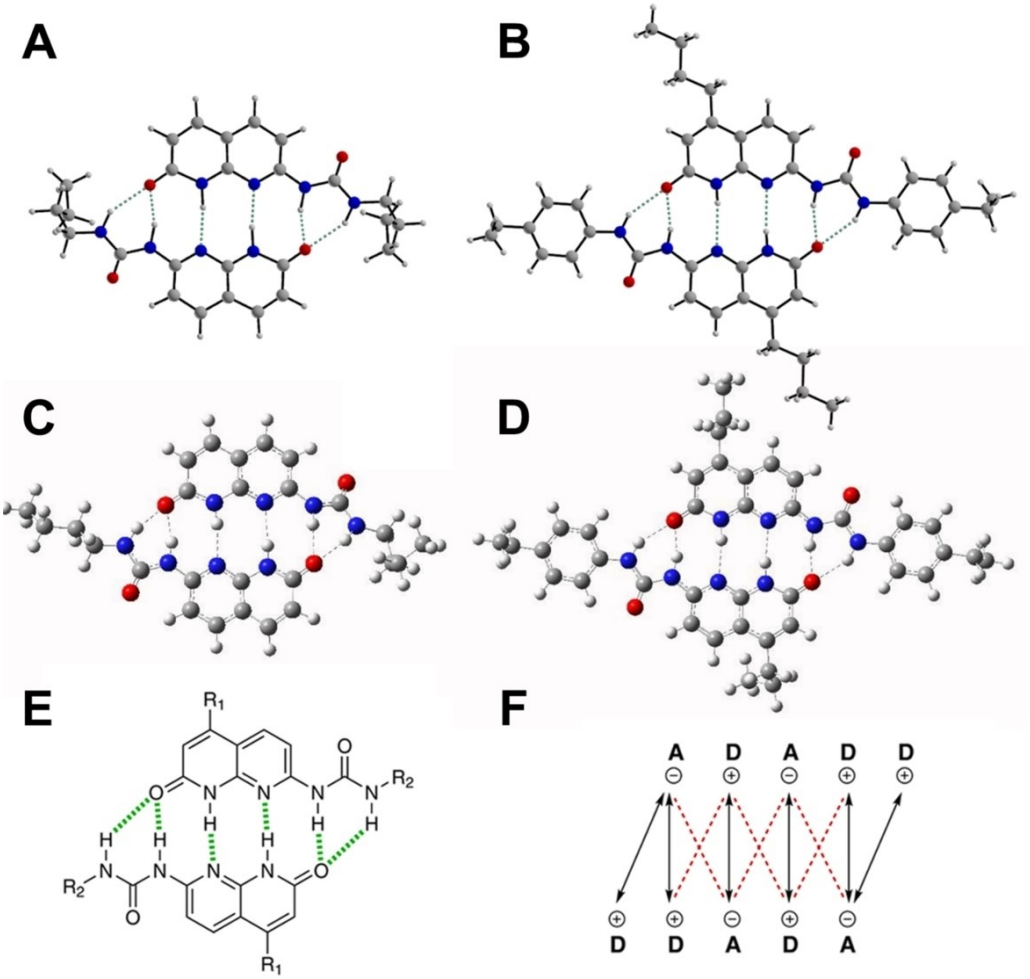

Figure 1. Dimeric assembly of A) **ODIN-But** and B) **ODIN-EtPh** in crystals grown from a $CHCl_3$ solution and obtained by Molecular Dynamics simulation C) **ODIN-But** and D) **ODIN-EtPh** performed in chloroform (See Computational Section and Supporting Information). The hydrogen bonds are highlighted with dashed lines. Oxygen atoms are represented in red, nitrogen in blue, carbon in light grey and hydrogen in white. E) Representation of the H-bonded dimeric assembly of **ODIN** molecules in a DDADA arrangement. The hydrogen bonds are represented as dotted lines (intramolecular, green; intermolecular, orange). (F) The schematization of hydrogen bond donor, D, and acceptor, A, in which the secondary repulsive electrostatic interactions are illustrated as red dashed lines.

Table 1. Spectroscopic data relative to ODIN-EtPh and ODIN-But in DMSO and $CHCL_3$. [a] Referred to diluted spectrum reported in Figure S14.

Molecule	Solvent	λ^{abs}_{max} [nm]	$\varepsilon_{(\lambda_{max})}$ [l/(M cm)]	λ^{em}_{max} [nm]	Φ	τ [ns]	k_r [ns^{-1}]
ODIN-EtPh	DMSO	363	28153	368	0.06	2.5	0.024
	$CHCl_3$	338		377	0.02	1.7	0.012
ODIN-But	DMSO	359	22368	383	0.78	2.1	0.37
	$CHCl_3$	339		377	0.47[a]	1.9	0.25

Absorption and emission spectra in DMSO of both compounds (top panels) show a well-resolved vibronic structure and a weak Stokes shift. The excitation spectrum is almost perfectly superimposed with the absorption one, an indication that in solution only one emissive species is present. The striking difference between **ODIN-EtPh** and **ODIN-But** regards the fluorescence quantum yield: **ODIN-EtPh** is a weak emitter, having $\phi \sim 6\%$, while **ODIN-But** is a very good emitter with $\phi \sim 78\%$. However, the variation of fluorescence lifetime (time constant reported in Table 1, decay curves in Figure S16) in DMSO between **ODIN-But** and **ODIN-EtPh** is negligible, translating into a 15-fold factor decrease of k_r in DMSO between **ODIN-EtPh** to **ODIN-But**, suggesting a sizeable decrease of the transition dipole moment.

TD-DFT calculations were run to investigate the different spectroscopic properties (technical details in the Supporting Information) of the two compounds. Ground-state optimization at the DFT level reveals that two structures are accessible for

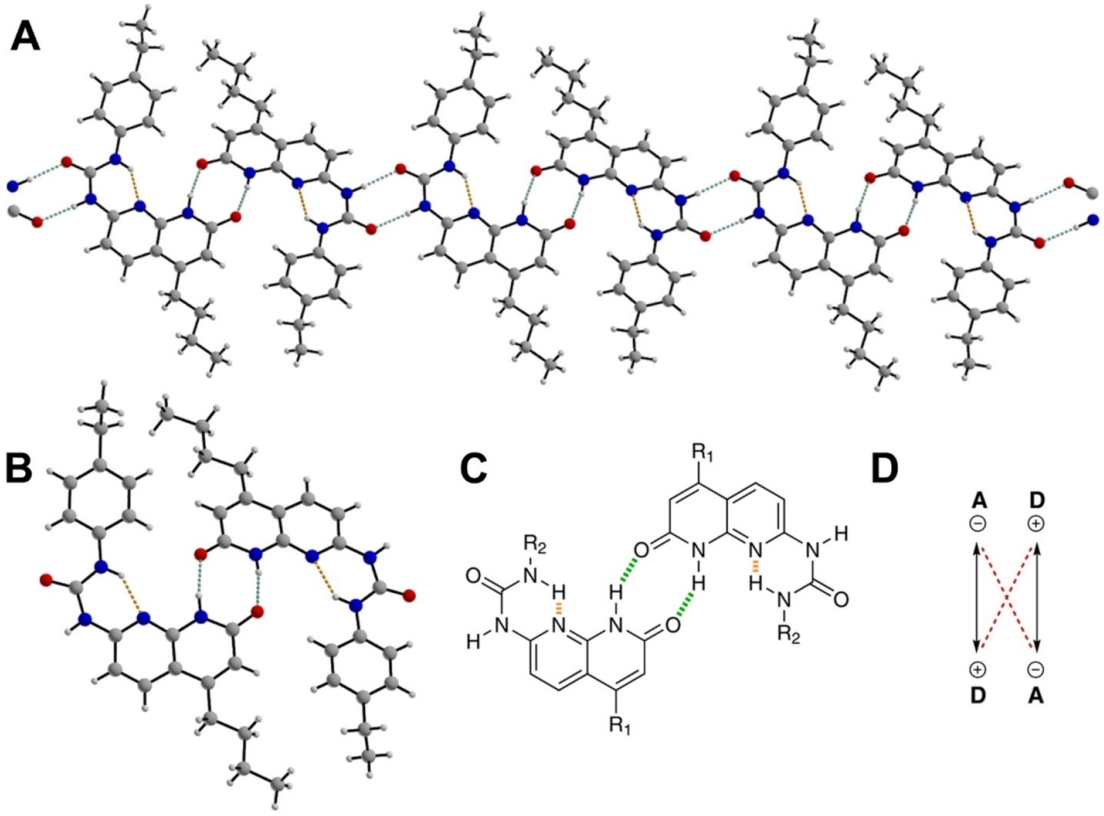

Figure 2. Dimeric assembly of A, B) **ODIN-EtPh** in crystals grown from a DMSO solution. The intramolecular and intermolecular hydrogen bonds are respectively highlighted with orange and green dashed lines. Oxygen atoms are represented in red, nitrogen in blue, carbon in light grey and hydrogen in white. C) Representation of the H-bonded dimeric assembly of **ODIN** molecules in a DA arrangement. The hydrogen bonds are represented as dotted lines (intramolecular, green; intermolecular, orange). D) The schematization of hydrogen bond donor, D, and acceptor, A, in which the secondary repulsive electrostatic interactions are illustrated as red dashed lines.

both compounds: a bent and a linear structure (Section 4.1 Supporting Information Figure S9). The bent structure is stabilized by an intramolecular H-bond, and is expected to be the dominant structure at room temperature (more details are reported in Supporting Information). Table S2 reports the results of TD-DFT calculations on the bent and linear structure for both compounds. For **ODIN-But**, bent and linear conformations have very similar spectroscopic properties: the first transition has a sizeable oscillator strength, and is dominated by a HOMO-LUMO transition, mostly localized on the naphtyridine moiety (Figure S10 in Supporting Information).

The excited state landscape is different for the two conformations of **ODIN-EtPh**: in the linear conformation the first excited state has a sizeable oscillator strength (0.63), while in the bent conformation the oscillator strength decreases by a six-fold factor. Furthermore, the transition energy shifts to the red and the second excited state acquires a relevant oscillator strength. Looking at the molecular orbital contributions to the first excited state of the linear conformation of **ODIN-EtPh**, we notice a sizeable charge transfer (CT) from the phenyl-urea to the naphtyridine unit (Figure S10), that is almost absent in **ODIN-But**. More interestingly, in the bent form of **ODIN-EtPh** the first excited state still has HOMO-LUMO character, but now the HOMO is localized mostly on the phenylurea moiety, while the LUMO is still on the naphtyridine moiety, conferring an almost pure CT character to the transition, with consequent decrease of the oscillator strength (from 0.63 in the linear form to 0.11 upon bending). The different nature of low energy excited states of bent **ODIN-EtPh** and **ODIN-But** is the key to rationalize the difference in quantum yields and the radiative constant k_r (Table 1).

Absorption spectra of **ODIN-EtPh** and **ODIN-But** collected in $CHCl_3$ (Figure 3, bottom panels) show different band-shapes with respect to absorption spectra in DMSO. The two peaks at ≈340 nm and ≈360 nm do not resemble a vibronic structure. The marked differences observed between absorption and excitation spectra (black and green lines) points to the presence of different species in solution, which can be reasonably attributed to the formation of aggregates. In fact, as shown in Figure S14, the absorption spectrum of **ODIN-But** changes in shape upon dilution, and the absorption spectrum of the diluted solution compares better with the spectral shape in DMSO.

No significant spectroscopic effects are observed for **ODIN-EtPh** upon dilution, suggesting that intermolecular interactions are stronger in aggregates of **ODIN-EtPh** than **ODIN-But**.

The variation of fluorescence lifetime in DMSO between **ODIN-But** and **ODIN-EtPh** is slightly observable, whereas the

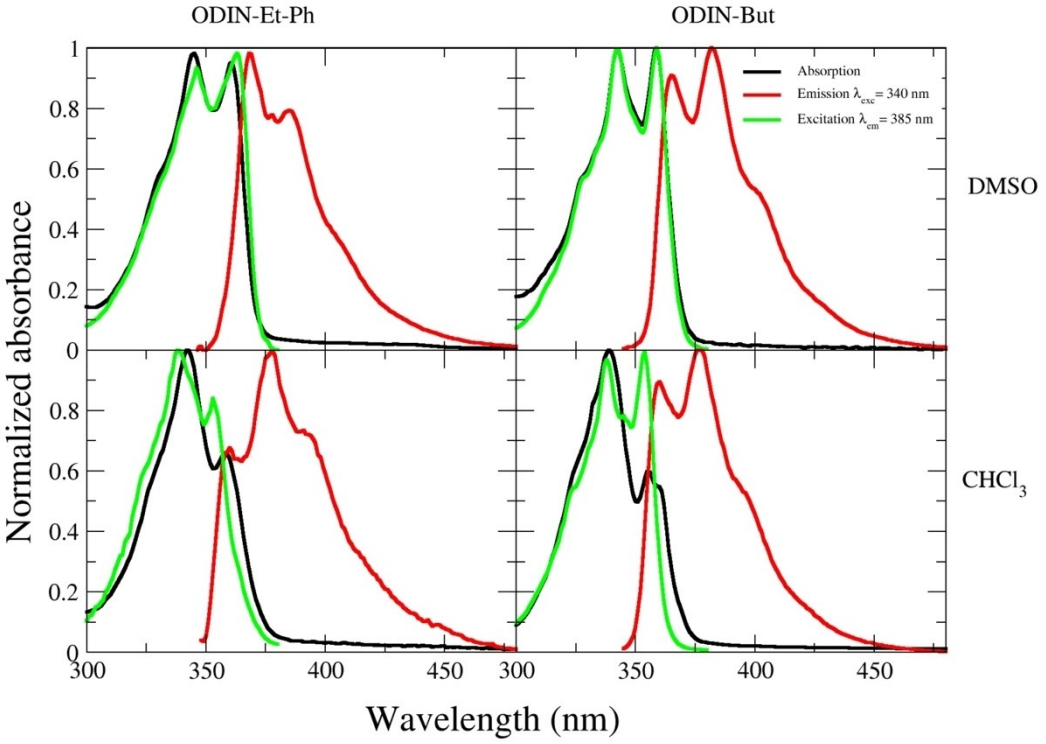

Figure 3. Absorption (black), emission (red) and fluorescence excitation (green) spectra of **ODIN-EtPh** (left) and **ODIN-But** (right) in DMSO (upper panels) and $CHCl_3$ (lower panels). Concentration of the DMSO solutions are: **ODIN-EtPh** 2.84×10^{-6} M, **ODIN-But** 3.13×10^{-6} M. The Concentrations of the $CHCl_3$ solutions are **ODIN-EtPh** 3.55×10^{-5} M, **ODIN-But**$\sim10^{-4}$ M.

quantum yields differ by a 13 factor (Table 1. This translates into a 15-fold factor decrease of k_r in DMSO between **ODIN-EtPh** to **ODIN-But**. This behavior suggests that an additional deactivation pathway, possibly involving different structural conformers, is present for **ODIN-EtPh** with respect to **ODIN-But** even in a polar solvent where aggregation is disfavored. To investigate the excited state dynamics we performed ultrafast transient absorption measurements.

Aggregation MD simulations

Aggregation in $CHCl_3$ is also confirmed by molecular dynamics (MD) simulations. MD calculations (Supporting Information, Section 4.1 for details) show that both **ODIN-EtPh** and **ODIN-But** in chloroform tend to aggregate in stable dimers showing a well-defined scheme of hydrogen bonding similar to that found in the crystal obtained from the same solvent (Figure 1). On the other hand, MD simulations confirm both **ODIN-But** and **ODIN-EtPh** remain in monomeric form in DMSO, starting either from a bent or linear conformation. Dimer stability is evidenced by the evolution of the inter-chromophores distance as a function of the simulation time reported in Figure S12 for **ODIN-EtPh**. Exploiting a counterpoise calculation, we obtained the stabilization energy of the array of hydrogen bonds formed in the dimer (6 hydrogen bonds, four being bifurcate) as $\Delta E_{stab} = E_{dimer} - 2E_{monomer}$, finding 192 kJ/mol stabilization for the dimer of **ODIN-EtPh** and 179.5 kJ/mol stabilization for **ODIN-But**. Calculations seem to qualitatively corroborate the experimental observation that **ODIN-EtPh** aggregates are more strongly bound which makes them less sensitive to dilution. The reason resides in the higher acidity of ureidic NH protons which form stronger HB with the lactam C=O. In fact, bifurcate HBs formed by **ODIN-EtPh** are shorter and closer to linearity of the D–H—A angle.

Ultrafast spectroscopy

Excited state evolution has been characterized by ultrafast UV-Vis transient absorption spectroscopy (TAS) and ultrafast visible pump-infrared probe spectroscopy (TRIR). Time resolved infrared spectra and their analysis are reported in Supporting Information Section 5.4.

Transient absorption

Pump-probe transient absorption measurements have been performed with the experimental setup described in the Supporting Information. The data have been analyzed with a target analysis procedure, selecting for each measurement a kinetic scheme taking into account the presence of different conformers and aggregates in solution. The analysis results with the main spectral components are reported in Figure 4, while the raw data and further details about the fitting procedure by

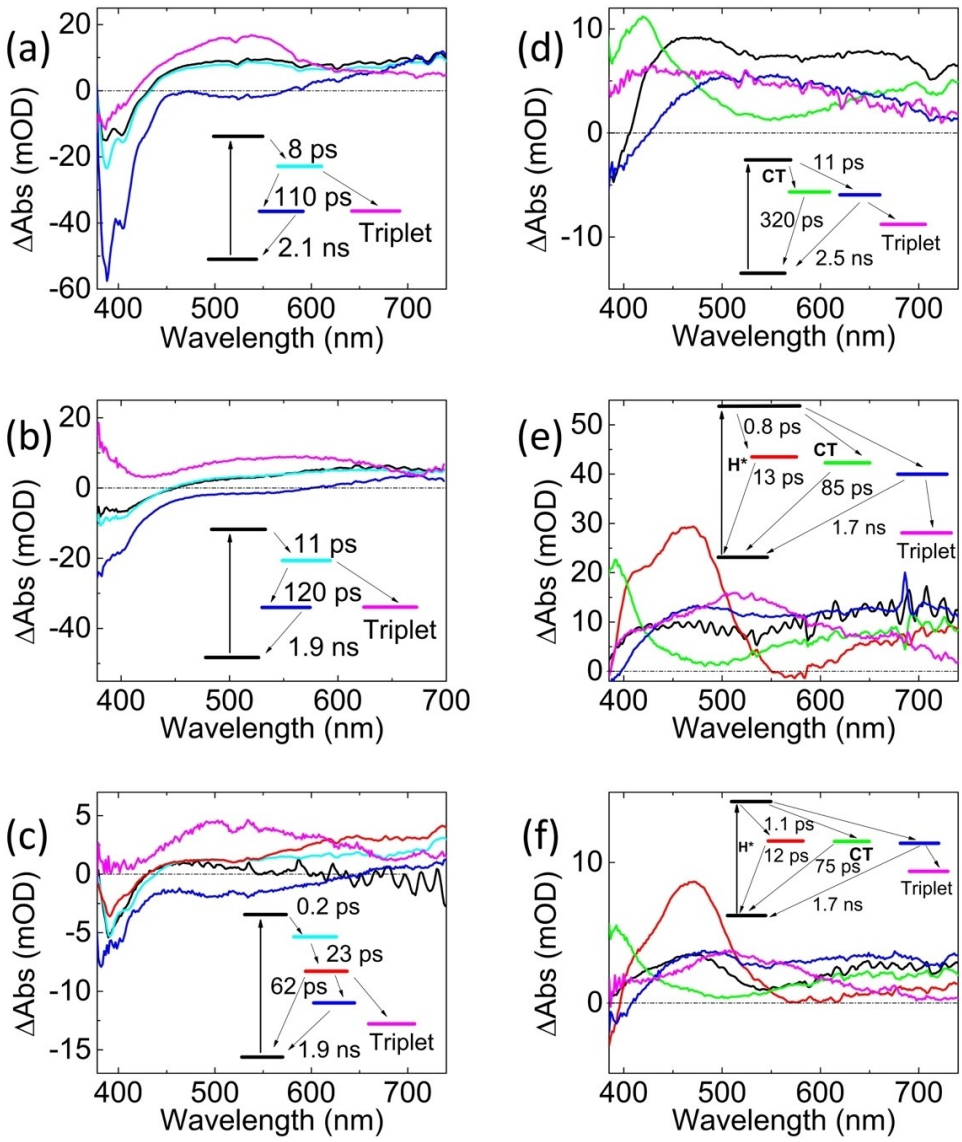

Figure 4. Target Analysis of the transient absorption spectra reported in Figure S17; a–c) **ODIN-But** and d–f) **ODIN-Et-Phen** in: a, d) DMSO following 350 nm excitation, b, e) in $CHCl_3$ following 350 nm excitation and c, f) 340 nm excitation. The kinetic models adopted are schematically represented inside the graph. Spectral components are reported in the main graphs; temporal evolution of each spectral component is reported in the inset.

target analysis are reported in the Supporting Information (Figures S17—S19).

The transient absorption spectra of **ODIN-But** in DMSO are characterized by a bleaching plus Stimulated Emission (SE) signal on the low-wavelength side of the spectrum and by a broad absorption band that covers the entire range between 450 nm and 750 nm. Measurements have been performed with 340 nm (see Supporting Information) and 350 nm excitation wavelength and the results obtained are almost superimposable. The temporal evolution has been fitted by using the dedicated target kinetic model reported in Figure 4(a). We assumed, as it was evidenced by the simulations, that the solution is formed by a mixture of bent (70—80%) and linear (30—20%) monomer molecules in the ground state. Both bent and linear species contribute to the black spectral component of Figure 4(a). Such spectrum evolves with a time constant of 8 ps in the red spectrum. The time scale and the spectral changes (slight narrowing) are fully compatible with a vibrational cooling. At this point we consider a branched evolution, giving rise to the blue and the magenta spectral components. Such bifurcated evolution is related to a) the linearization of a small fraction of bent molecules (inducing a slight increase of the stimulated emission signal (blue spectral component) and b) to the population of the magenta long living excited state (possibly a triplet state). Finally, the blue component relaxes back to the ground state through fluorescence emission.

Concerning **ODIN-EtPh** in DMSO, the most significant feature is a "transient decrease" in the intensity of the bleaching plus stimulated emission signal (see Figures S17f and S19f) on the hundreds picoseconds time scale, intensity partially recovered around one nanosecond. This "transient decrease" is due to the superimposition of an excited state absorption, that

decays in the hundred picoseconds time scale, on the stimulated emission. Target kinetic model is reported in Figure 4(d) and is based, as for **ODIN-But** on the results of computations, indicating the species present at the ground state. The first spectral component (black Figure 4d) is ascribed to the presence of two excited species: bent molecules (80—90%) and a small fraction of linear molecules (20—10%). On the picosecond time scale, the excited bent molecules undergo relaxation towards an excited state showing the transient absorption depicted in green in Figure 4(d). Based again on the results of computations, this state has been assigned to the Charge-Transfer and not emissive state (**CT**). On the same time scale, linear molecules cool down giving rise to the blue spectrum (in **ODIN-But** the cooling process was observed on the 8 ps time scale). The **CT** relaxes back to the ground state with a time constant of 302 ps while the emissive state of linear molecules undergoes a partial population transfer to a long-living state (possibly a triplet state, magenta component in Figure 4d) and the back relaxation to the ground state.

The excited state evolution of **ODIN-But** in $CHCl_3$ excited at 350 nm (Figure 4b) very well traces the trend observed for the **ODIN-But** in DMSO and the target analysis follows the same kinetic model. On the contrary the excitation at 340 nm (Figure 4c) shows a different excited state absorption pathway. When **ODIN-But** is pumped at 340 nm, the dimeric form it is preferentially excited. The bright excitonic state of the dimer highly contributes to the black spectral component in Figure 4(c). The red spectral component is assigned in terms of different contributions: broad absorption and stimulated emission from the monomer species and an excited state absorption on the red part of the spectrum, from the dark excitonic state (**H***) of dimers. The state **H*** than relaxes back to the ground state on several tens of picoseconds timescale ($\tau = 62$ ps), leaving the residual spectral contribute from the monomeric species (blue and magenta spectral components in Figure 4c), similar to the monomer species in DMSO (blue and magenta spectral component in Figure 4a).

Excited state absorption spectra of **ODIN-EtPh** in $CHCl_3$ evidence a different pattern, independently from the excitation wavelength. The main spectral feature is a well-structured excited state absorption spanning the 400–500 nm spectral range (red spectral component Figure 4e, f). It is formed with a time constant of roughly 1–2 ps, and decays to the ground state with a time constant of 10–11 ps. It has been assigned to the transient absorption from the dark exciton state (**H***) of the dimer. The time scale for the formation, as well as its decay time are in reasonable agreement with the excited state evolution observed for the excitonic states of some Perylene-dicarboximide (PDI) derivatives.[28][29][30] A small percentage of monomers in the ground state cannot be excluded, giving rise to the characteristic **CT** excited state absorption (green spectral component in Figure 4e, f) that relaxes back to the ground state with time constants of 85 ps ($\lambda_{exc} = 350$ nm) and 75 picoseconds ($\lambda_{exc} = 340$ nm). Furthermore, it is worth mentioning that a residual signal, not fully recovering on our accessible maximum temporal delay time (1.5–1.6 ns), is observed (see the fitted kinetic traces reported in Figure S19 Supporting Information). Careful target analysis allowed us to disentangle two different contributions: namely the blue and the magenta spectral component reported in Figure 4(e and f). The spectral shape (Figure 4e, f) of blue component very well matches, spectrally and temporally, the blue nanoseconds decaying component observed in DMSO (Figure 4d), leading us to assign such component as the emissive one. The long living component, represented by the magenta spectra in Figure 4(e, f) and that does not decay on our accessible time scale, very well resembles the magenta spectrum obtained from the target analysis of **ODIN-But** in $CHCl_3$ after 340 nm excitation, suggesting the population of a triplet state also for **ODIN-EtPh**. Further information on the excited state dynamics is obtained from the analysis of transient absorption data in the infrared (see SI: FTIR in Figure S20, time resolved data in Figure S21–S24 and discussion there reported). These data confirm the dynamic evolution observed in the visible for both molecules, and further suggest that the systems do not undergo any conformational change, supporting the observation that the different conformations-aggregates in solution do not interconvert between each other, but decay following independent pathways.

Conclusions

The ODIN motif object of this study is a functionalized naphthyridine unit designed to self-dimerize through intermolecular hydrogen bonds as demonstrated in the solid state through X-ray crystal structure analysis.

Crystals of **ODIN-EtPh** were obtained both from $CHCl_3$ and DMSO. However, while the crystals obtained from $CHCl_3$ evidenced dimerization by linear conformers of **ODIN-EtPh** with the formation of six intermolecular hydrogen bonds (Figure 1A, B), the crystals obtained from DMSO showed bent **ODIN-EtPh** conformers forming dimers with only two intermolecular and one intramolecular hydrogen bond (Figure 2A, B). Such experimental evidence is related to the strong hydrogen-bond acceptor properties of DMSO with respect to chloroform. MD simulation performed in chloroform strongly support the X-Ray evidence for both compounds, as shown in Figure 1(C, D).

In DMSO, **ODIN-EtPh** and **ODIN-But** exhibit distinct absorption and emission spectra, with **ODIN-But** showing high fluorescence (φ~78%) and **ODIN-EtPh** being nearly non-emissive ($\varphi < 6\%$). MD simulations showed that **ODIN-But** and **ODIN-EtPh** are stable as monomer in DMSO. The fluorescence quenching in **ODIN-EtPh** is attributed to an intramolecular distortion leading to the population transfer towards a non-emissive state during the relaxation process. Computational analysis reveals that **ODIN-EtPh** possesses an excited state, lower in energy than the bright state, with pronounced charge transfer character and a very low transition dipole. Transient absorption spectroscopy confirms these results, showing the presence of an excited electronic state that decays with a time constant of 320 ps. Finally, our data strongly indicate that both **ODIN-EtPh** and **ODIN-But** are present as monomer species in DMSO.

In $CHCl_3$, both **ODIN-EtPh** and **ODIN-But** display optical properties indicating intermolecular interactions. The absorption spectra for both compounds suggest the formation of H-type intermolecular aggregates. MD simulations support this evidence, indicating that **ODIN-But** and **ODIN-EtPh** form stable dimers in chloroform with the hydrogen bond pattern DDADA. However, the excitation spectra of **ODIN-But** are strongly concentration-dependent, while **ODIN-EtPh** shows little dependence, suggesting that **ODIN-EtPh** form more stable intermolecular interactions. On the other hand, for **ODIN-EtPh** we evidence the formation of a dark excitonic state on a timescale of 1–2 picoseconds, which decays back to the ground state on a timescale of 10–11 picoseconds, further contributing to the quenching of fluorescence emission.

This study highlights the selective effect of multiple hydrogen bonds on dimer formation and the influence of the substituent attached to the ureidic group. The presence of a phenyl group stabilizes the aggregates, as demonstrated by the strong dependence of **ODIN-But**'s excitation spectra on concentration, as compared to **ODIN-EtPh**. Additionally, the introduction of a phenyl group leads to the formation of charge transfer excited states, altering the distribution of excited electronic states in the molecules.

Supporting Information

The authors have cited additional references within the Supporting Information.[31–43]

Acknowledgements

A.I., C.S. and F.B. would like to acknowledge European Union support Through the Micro4Nano project, within the European Union's Horizon 2020 research and innovation program, under the Marie Skłodowska-Curie grant agreement No 101007804. A.L. would like to acknowledge the support of Fondazione Cassa di Risparmio di Torino (CRT) through the Visco3DCell project. A.L., F.B. and C.S. would like to acknowledge Gioele Genovese for the very preliminary investigation performed on such molecules. We thank the Centro Interfacoltà di Misure "G. Casnati" of the University of Parma for the use of NMR and HR-MS facilities. This work benefited from the equipment and framework of the COMP-R Initiative, funded by the Departments of Excellence program of the Italian Ministry for Education, University and Research (MIUR, 2023–2027). E.D. and R.P. would like to thank the support of PNRR – M4C2 – I1.1 – PRIN 2022 REPRONET (2022TCJRCA) financed by NextGenerationEU. AL, MDD,SD would like to thank the support of the EU Horizon 2020 research and innovation program under grant agreement 871124 Laserlab-Europe.

Conflict of Interests

The authors declare no conflict of interest.

Data Availability Statement

The data that support the findings of this study are available from the corresponding author upon reasonable request.

Keywords: hydrogen bond · H-Aggregate · ultrafast pump-probe · electron diffraction · fluorescence

[1] A. Datta, S. K. Pati, *Chem. Soc. Rev.* **2006**, *35*, 1305–1323.
[2] C. Liu, Z. Liu, X. Yin, G. Wu, *Macromolecules* **2015**, *48*, 4196–4206.
[3] J. X. Chen, H. Wang, Y. F. Xiao, K. Wang, M. H. Zheng, W. C. Chen, L. Zhou, D. Hu, Y. Huo, C. S. Lee, X. H. Zhang, *Small* **2022**, *18*, 202201548.
[4] Y. Tang, Y. Liu, W. Ning, L. Zhan, J. Ding, M. Yu, H. Liu, Y. Gao, G. Xie, C. Yang, *J. Mater. Chem. C* **2022**, *10*, 4637–4645.
[5] U. Ray, Z. Pang, T. Li, *J. Appl. Phys.* **2022**, *132*, 210703.
[6] L. Jiang, J. Gao, Y. Fu, H. Dong, H. Zhao, H. Li, Q. Tang, K. Chen, W. Hu, *Nanoscale* **2010**, *2*, 2652–2656.
[7] N. R. Ávila-Rovelo, A. Ruiz-Carretero, *Organic Materials* **2020**, *02*, 47–63.
[8] J. Heo, D. P. Murale, H. Y. Yoon, V. Arun, S. Choi, E. Kim, J. Lee, S. Kim, *Aggregate* **2022**, *3*, e159.
[9] N. J. Hestand, F. C. Spano, *Chem. Rev.* **2018**, *118*, 7069–7163.
[10] D. M. Eisele, D. H. Arias, X. Fu, E. A. Bloemsma, C. P. Steiner, R. A. Jensen, P. Rebentrost, H. Eisele, A. Tokmakoff, S. Lloyd, K. A. Nelson, D. Nicastro, J. Knoester, M. G. Bawendi, *Proc. Natl. Acad. Sci. USA* **2014**, *111*, E3367–E3375.
[11] C. D. Bösch, S. M. Langenegger, R. Häner, *Angew. Chem. Int. Ed.* **2016**, *128*, 10115–10118.
[12] S. Doria, M. Di Donato, R. Borrelli, M. F. Gelin, J. Caram, M. Pagliai, P. Foggi, A. Lapini, *J. Mater. Chem. C* **2022**, *10*, 7216–7226.
[13] D. M. Eisele, C. W. Cone, E. A. Bloemsma, S. M. Vlaming, C. G. F. Van Der Kwaak, R. J. Silbey, M. G. Bawendi, J. Knoester, J. P. Rabe, D. A. Vanden Bout, *Nat. Chem.* **2012**, *4*, 655–662.
[14] M. Shirakawa, S. ichiro Kawano, N. Fujita, K. Sada, S. Shinkai, *J. Org. Chem.* **2003**, *68*, 5037–5044.
[15] C. A. Hunter, H. L. Anderson, *Angew. Chem. Int. Ed.* **2009**, *48*, 7488–7499.
[16] L. L. Parker, A. R. Houk, J. H. Jensen, *J. Am. Chem. Soc.* **2006**, *128*, 9863–9872.
[17] Y. Zhou, G. Deng, Y. Z. Zheng, J. Xu, H. Ashraf, Z. W. Yu, *Sci. Rep.* **2016**, *6*, 36932.
[18] B. A. Blight, C. A. Hunter, D. A. Leigh, H. McNab, P. I. T. Thomson, *Nat. Chem.* **2011**, *3*, 244–248.
[19] W. L. Jorgensen, J. Pranata, *J. Am. Chem. Soc.* **1990**, *112*, 2008–2010.
[20] J. Tellers, S. Canossa, R. Pinalli, M. Soliman, J. Vachon, E. Dalcanale, *Macromolecules* **2018**, *51*, 7680–7691.
[21] M. Golkaram, L. Boetje, J. Dong, L. E. A. Suarez, C. Fodor, D. Maniar, E. Van Ruymbeke, S. Faraji, G. Portale, K. Loos, *ACS Omega* **2019**, *4*, 16481–16492.
[22] M. Gemmi, E. Mugnaioli, T. E. Gorelik, U. Kolb, L. Palatinus, P. Boullay, S. Hovmöller, J. P. Abrahams, *ACS Cent. Sci.* **2019**, *5*, 1315–1329.
[23] M. Gemmi, A. E. Lanza, *Acta Crystallogr. Sect. B* **2019**, *75*, 495–504.
[24] I. Nederlof, E. Van Genderen, Y. W. Li, J. P. Abrahams, *Acta Crystallogr. Sect. D* **2013**, *69*, 1223–1230.
[25] T. Yang, H. Xu, X. Zou, A. Borbély, *J. Appl. Crystallogr.* **2022**, *55*, 1583–1591.
[26] F. Bertocchi, A. Delledonne, G. Vargas-Nadal, F. Terenziani, A. Painelli, C. Sissa, *J. Phys. Chem. C* **2023**, *127*, 10185–10196.
[27] A. Delledonne, J. Morla-Folch, M. Anzola, F. Bertocchi, G. Vargas-Nadal, M. Köber, C. Sissa, N. Ventosa, A. Painelli, *J. Mater. Chem. C* **2021**, *9*, 10952–10964.
[28] K. E. Brown, W. A. Salamant, L. E. Shoer, R. M. Young, M. R. Wasielewski, *J. Phys. Chem. Lett.* **2014**, *5*, 2588–2593.
[29] J. M. Giaimo, J. V. Lockard, L. E. Sinks, A. M. Scott, T. M. Wilson, M. R. Wasielewski, *J. Phys. Chem. A* **2008**, *112*, 2322–2330.
[30] A. E. Clark, C. Qin, A. D. Q. Li, *J. Am. Chem. Soc.* **2007**, *129*, 7586–7595.
[31] B. Bardi, D. Giavazzi, E. Ferrari, A. Iagatti, M. Di Donato, D. K. A. Phan Huu, F. Di Maiolo, C. Sissa, M. Masino, A. Lapini, A. Painelli, *Mater. Horiz.* **2023**, advance article.
[32] P. Tourón Touceda, S. Mosquera Vázquez, M. Lima, A. Lapini, P. Foggi, A. Dei, R. Righini, *Phys. Chem. Chem. Phys.* **2012**, *14*, 1038–1047.
[33] J. J. Snellenburg, S. Laptenok, R. Seger, K. M. Mullen, I. H. M. van Stokkum, *J. Stat. Softw.* **2012**, *49*, 1–22.

[34] J. Wang, R. M. Wolf, J. W. Caldwell, P. A. Kollman, D. A. Case, *J. Comput. Chem.* **2004**, *25*, 1157–1174.
[35] J. Wang, W. Wang, P. A. Kollman, D. A. Case, *J. Mol. Graphics Modell.* **2006**, *25*, 247–260.
[36] M. J. Frisch, G. W. Trucks, H. B. Schlegel, G. E. Scuseria, M. A. Robb, J. R. Cheeseman, G. Scalmani, V. Barone, G. A. Petersson, H. Nakatsuji, X. Li, M. Caricato, A. V Marenich, J. Bloino, B. G. Janesko, R. Gomperts, B. Mennucci, H. P. Hratchian, J. V Ortiz, A. F. Izmaylov, J. L. Sonnenberg, D. Williams-Young, F. Ding, F. Lipparini, F. Egidi, J. Goings, B. Peng, A. Petrone, T. Henderson, D. Ranasinghe, V. G. Zakrzewski, J. Gao, N. Rega, G. Zheng, W. Liang, M. Hada, M. Ehara, K. Toyota, R. Fukuda, J. Hasegawa, M. Ishida, T. Nakajima, Y. Honda, O. Kitao, H. Nakai, T. Vreven, K. Throssell, J. A. Montgomery Jr., J. E. Peralta, F. Ogliaro, M. J. Bearpark, J. J. Heyd, E. N. Brothers, K. N. Kudin, V. N. Staroverov, T. A. Keith, R. Kobayashi, J. Normand, K. Raghavachari, A. P. Rendell, J. C. Burant, S. S. Iyengar, J. Tomasi, M. Cossi, J. M. Millam, M. Klene, C. Adamo, R. Cammi, J. W. Ochterski, R. L. Martin, K. Morokuma, O. Farkas, J. B. Foresman, D. J. Fox. *Gaussian, Inc., Wallingford CT*, **2016**.
[37] H. Bekker, H. J. C. Berendsen, E. J. Dijkstra, S. Acheterop, R. Vondrumen, D. Vanderspoel, A. Sijbers, H. Keegstra, M. K. R. Renardus, in *Physics Computing'92* (Eds.: R. A. DeGroot, J. Nadrchal), World Scientific Publishing, **1993**, pp. 252–256.
[38] E. Lindahl, B. Hess, D. van der Spoel, *J. Mol. Model.* **2001**, *7*, 306–317.
[39] W. Humphrey, A. Dalke, K. Schulten, *J. Mol. Graphics* **1996**, *14*, 33–38.
[40] L. Palatinus, P. Brázda, M. Jelìnek, J. Hrdá, G. Steciuk, M. Klementová, *Acta Crystallogr. Sect. B* **2019**, *75*, 512–522.
[41] G. M. Sheldrick, *Acta Crystallogr. Sect. A* **2008**, *64*, 112–122.
[42] O. V. Dolomanov, L. J. Bourhis, R. J. Gildea, J. A. K. Howard, H. Puschmann, *J. Appl. Crystallogr.* **2009**, *42*, 339–341.
[43] G. M. Sheldrick, *Acta Crystallogr. Sect. A* **2015**, *71*, 3–8.

Manuscript received: August 10, 2023
Accepted manuscript online: October 3, 2023
Version of record online: November 13, 2023